

Application of MTO-thyristors in Current Stiff Converters with Resonant Snubbers

Braz J. Cardoso Filho
Universidade Federal de Minas Gerais
Depto. Engenharia Eletrica
Av. Antonio Carlos, 6627
Belo Horizonte, MG 31270-010 - Brazil

Thomas A. Lipo
University of Wisconsin-Madison
Dept. Electrical and Computer Engineering
1415 Engineering Dr.
Madison, WI 53706

Abstract— This paper addresses the impact of power devices switching characteristics on design and performance of pulse width modulated current stiff converter (CSC) topologies with resonant snubbers. The MTO thyristors were selected for this study due to their high voltage and current ratings, simplified gate drive circuitry, unity gain turn-off, greatly reduced storage time allowing higher switching frequencies, and reverse voltage blocking capability. The analysis presented in this paper is supported by experimental data obtained from a CSC commutation cell capable of reproducing all the commutation processes in the current stiff converter topologies with active resonant snubbers. Issues involved in the implementation of the commutation cell itself and MTO characteristics relevant for their operation in CSC topologies with resonant snubbers are addressed in detail in this paper.

I. INTRODUCTION

Resonant snubbers [1] have recently been proposed for improvement of the performance of PWM Current Stiff Converters (CSC) [2], [3], [4]. Among the advantages of resonant snubbers when compared to classical LRCD snubbers [5] and regenerative schemes [6], one can point out: essentially lossless structure, intrinsic minimization of stray inductances improving device utilization, reasonably low parts count and hardware complexity. On the other hand, resonant snubbers are active circuits and require control for proper operation.

Resonant snubber design goals are minimization of the switching losses while constraining voltage and current stresses on the main switches and snubber components. The design of the resonant snubber components is then greatly dependent on the switching characteristics of the main power devices employed in the CSC. In this paper, high power MTO thyristors [7] were investigated for application in CSC topologies with resonant snubbers. These new devices present improved turn-off characteristics, simplified gate drive requirements, unity gain turn-off, short storage time ($\approx 1 \mu s$) and reverse voltage blocking capability. Other high power devices such as the IGCTs and HV-IGBTs are also interesting possibilities, mainly if a series diode is introduced in the device package to add reverse voltage blocking capability.

The analysis presented in this paper is supported by experimental results obtained from a commutation cell capable of reproducing all the commutation processes corresponding to current stiff converter topologies with resonant

snubbers [1], [2], [3], [4]. This commutation cell is based on the MTO XSDM170HK (4500 V/500 A) [8]. Issues involved in the implementation of the commutation cell itself as well as the MTO-thyristor characteristics relevant for the operation in CSC topologies with resonant snubbers are addressed in detail in this paper.

II. OVERVIEW OF MTO-THYRISTOR CHARACTERISTICS

A. Forward bias

The MTO gate turn-off process is based on the introduction of a very low impedance ($r_{DS_{on,eq}}$ of the MOSFETs in the device) in parallel with the junction j_3 , as shown in fig. 1. With the MOSFETs on, the gate current changes polarity and increases rapidly in the negative direction. In this process, the charge stored in the P -base is eliminated in a short interval (storage time) and junction j_3 stops conducting. At this point the NPN transistor in the MTO structure is off and the PNP transistor enters an open-base turn-off process. The MTO is held in the off state provided that $r_{DS_{on,eq}}$ of the MOSFETs in the device is sufficiently low. The upper limit on the equivalent on-state resistance of the MOSFETs and P -base is obtained from (1) [9]:

$$i_A \leq \frac{V_{bi}}{r_{DS_{on,eq}} + r_{P-base,eq}} \quad (1)$$

where $r_{DS_{on,eq}}$ is the equivalent on-state resistance of the MOSFETs, $r_{P-base,eq}$ is the equivalent lateral resistance of the P -base region, V_{bi} is the built in potential across the gate-cathode junction and i_A is the anode current to be turned-off.

The MTO dV/dt capability is also a function of the total gate-cathode resistance in the off-state. Low equivalent P -base and on-state MOSFET resistances are required to prevent the displacement current associated with the change in the width of the drift region to forward bias junction j_3 and trigger the device into conduction. This situation is particularly important at high forward blocking voltages [10]. It is also interesting to note that in the off-state, the MTO structure is similar to that of regular thyristors with emitter shorts. The reduced dependence of the forward breakdown voltage on the temperature, from the reduction of the current gain α_{NPN} at low current levels, is also expected here.

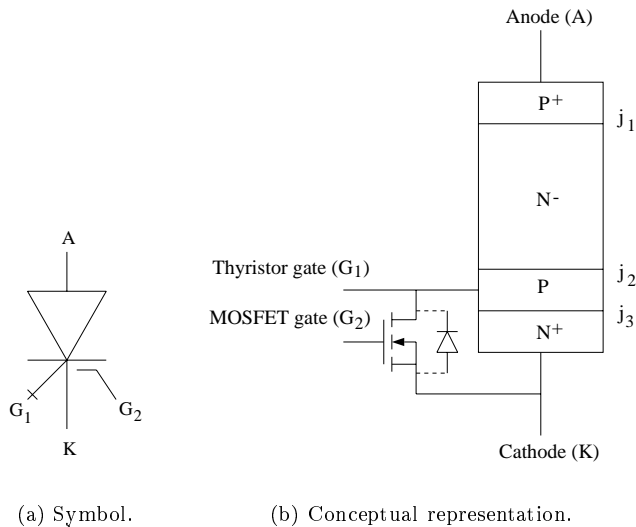


Fig. 1. MTO Thyristor.

The situations pointed out above suggest that a fairly low $r_{P-base,eq}$ is proper of MTO thyristors, yielding a low gate-cathode resistance in the off-state. However, a reduction in the equivalent $P-base$ resistance can potentially degrade the on-state characteristics of the device. For instance, larger front-porch and back-porch gate current requirements are expected as a result of low $r_{P-base,eq}$ [10].

The voltage driving the negative gate current in the MTOs during the turn-off process is the voltage across the gate-cathode junction of the thyristor part of the device (v_{j_3}). This low driving voltage combined to stray inductances in the turn-off path of the gate current increase the chances for non-homogeneous turn-off, particularly at higher anode currents. Low driving voltage and stray inductances also contribute to non-uniform current sharing among the multiple parallel MOSFETs in the turn-off path of the gate current.

B. Reverse bias

MTOs are switched from the conduction mode to the reverse blocking mode by negative anode voltage, through a zero current turn-off process similar to that observed in regular thyristor devices. Notice, however, that the intrinsic reverse diodes across the turn-off MOSFETs in the MTO structure constrain the reverse voltage across junction j_3 , such that $v_{j_3} > 0$. As a result, no reverse voltage breakdown takes place across junction j_3 .

Under negative anode voltage, both PNP and NPN transistors in the device structure operate in the reverse bias mode. This situation implies that the MTO does not latch up under reverse anode voltage if positive current is injected into the turn-on gate terminal G_1 , with junctions j_2 and j_3 forward biased. The result of injection of positive current into G_1 is an increase of the reverse anode current. The device operates in the remote base transistor mode (active region) [11]. In this operating mode, the current gain $|i_A|/i_{G_1}$ is quite low, increasing in direct proportion

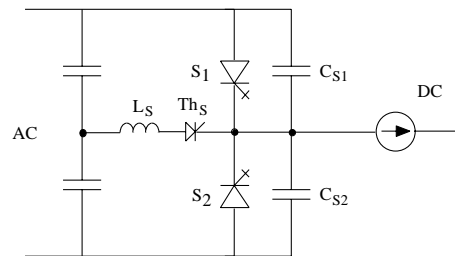


Fig. 2. Basic realizations of the resonant snubbers in CSC.

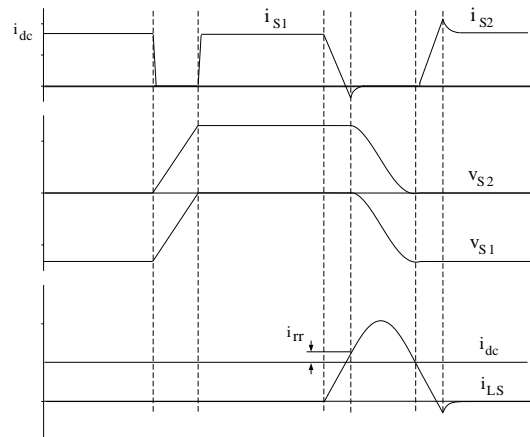


Fig. 3. Basic waveforms of the CSC with resonant snubbers.

to the anode voltage (the equivalent base transport factor rises as the width of the neutral region in the N-base is reduced).

III. COMMUTATION IN CSC TOPOLOGIES WITH RESONANT SNUBBERS

A. Realization and commutation sequences [2]

The basic implementation of the resonant snubbers with auxiliary switches for CSCs is depicted in fig. 2 [1]. The CSC realization requires one auxiliary device for each pair of main switches in the common-anode and common-cathode groups. A back-to-back arrangement of snubber devices, as in the VSC [1], [12] realization, can also be used to minimize the influence of the dc bus current on the commutation process.

Fig. 3 shows the relevant waveforms of the resonant snubber implementation in CSCs, where two commutation sequences can be identified. The *passive commutation sequence* takes place whenever the incoming switch is reverse biased. Otherwise, external means have to be provided to establish zero voltage conditions on the incoming switch during its turn-off process and the *active commutation sequence* takes place.

The passive commutation sequence starts when the conducting switch is turned off. The dc bus current commutates to the snubber capacitors and the voltage across the devices ramps up. The incoming switch starts conducting at the zero crossing of the voltage across its terminals.

The active commutation sequence is based on the introduction of a resonant mode to drive the voltage across the

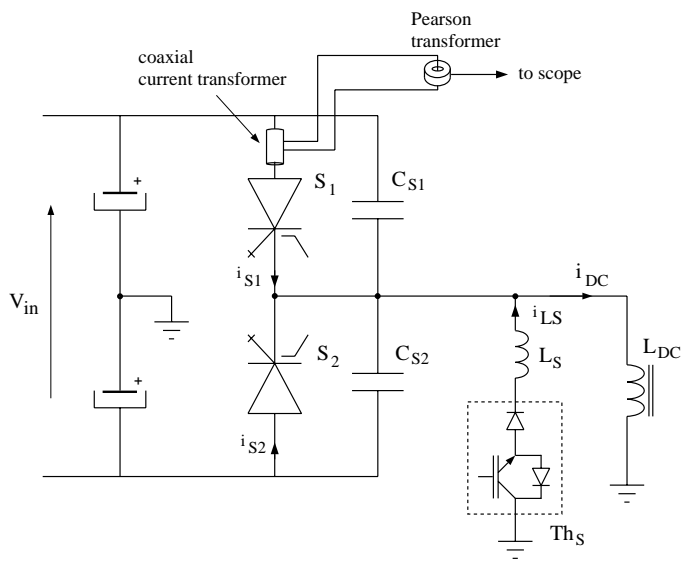


Fig. 4. High power (pulsed) test setup employing MTOs.

incoming switch down to zero. This sequence starts by turning on the snubber switch. The current through the snubber inductor ramps up, reaching the dc bus current amplitude. At this instant, the outgoing switch is turned off under zero current conditions. Since no switch is conducting, a resonant mode between the snubber inductor and capacitors takes place. The charge in the snubber capacitor across the incoming switch is transferred to the one across the outgoing switch (reverse biased) and the incoming switch turns on under zero anode voltage.

B. Test Setup

The high power (pulsed) test setup implemented for the evaluation of the resonant snubbers in CSC topologies is depicted in fig. 4, with MTO devices employed in the main switches (S_1 and S_2). A series connected IGBT and fast recovery diode set is employed as the snubber switch (Th_S).

The test circuit in fig. 4 is capable of reproducing both passive and active commutation sequences with minimum hardware and control complexity. In this circuit, the snubber driving voltage is set for *optimal* commutation conditions [2] with the snubber driving voltage derived from the center tap of the input supply V_{in} . *Near optimal* commutation conditions [3] can be set by introducing an independent supply to set the snubber driving voltage or by splitting the input voltage in multiple levels.

A cascade connection of two current transformers has been used to minimize the total insertion impedance associated with the measurement of the current through the devices. A co-axial current transformer was inserted directly in the power setup. This transformer employs a wound tape toroidal core (part number W783 50451-1/2D from MAGNETICS). The secondary winding consists of 10 turns of copper tape wound around the toroidal core. The primary side of the transformer was built by machining a toroidal shape with the proper dimensions to accommodate the transformer core and secondary winding in a copper

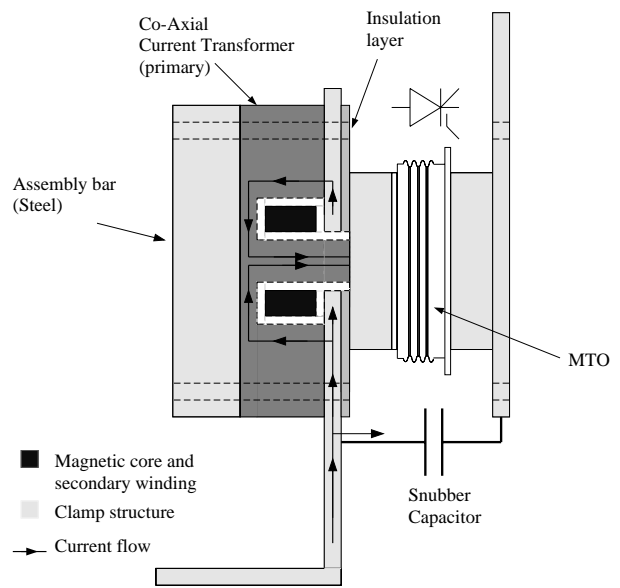


Fig. 5. Detail of the assembly of the co-axial current transformer.

bar. Fig. 5 shows a detail of the power setup illustrating the connection of the primary side of the co-axial current transformer to the power device. Notice that this arrangement allows the measurement of the current through the power device only and does not include the snubber capacitor current. The current through the shorted secondary winding of the co-axial transformer is then measured using a commercial current transformer (PEARSON 411). The total gain of the cascade connection is 0.01 V/A (1 M Ω input impedance).

The operation of the test setup is illustrated by the idealized waveforms depicted in fig. 6. Passive commutation processes take place at instants t_1 and t_3 . Active commutation process is observed at instant t_2 . Fig. 6 also shows the commands for all the switches in the circuit.

The commutation cell described here was tested for several values of dc bus current, input voltage and snubber capacitor values in order to identify trade-offs in CSC operation involving these quantities. The following paragraphs present the procedures and summarize the results obtained in this investigation.

C. Passive Commutation

Typical passive commutation waveforms illustrating the entire switching transient are shown in fig. 7, where commutation takes place from switch S_1 to switch S_2 . These plots were obtained with $i_{dc} = 150$ A, $V_{in} = 750$ V and $C_S = 1.0$ μ F. While the turn-off process is similar to that observed in VSC topologies, the turn-on process implies reverse bias on the incoming switch and it is proper of CSC topologies employing self-commutated devices.

C.1 Turn-Off process issues

The turn-off loss in the passive commutation sequence is the main figure in the design of the snubber capacitors. The lossless reset mechanism provided by the resonant snubber

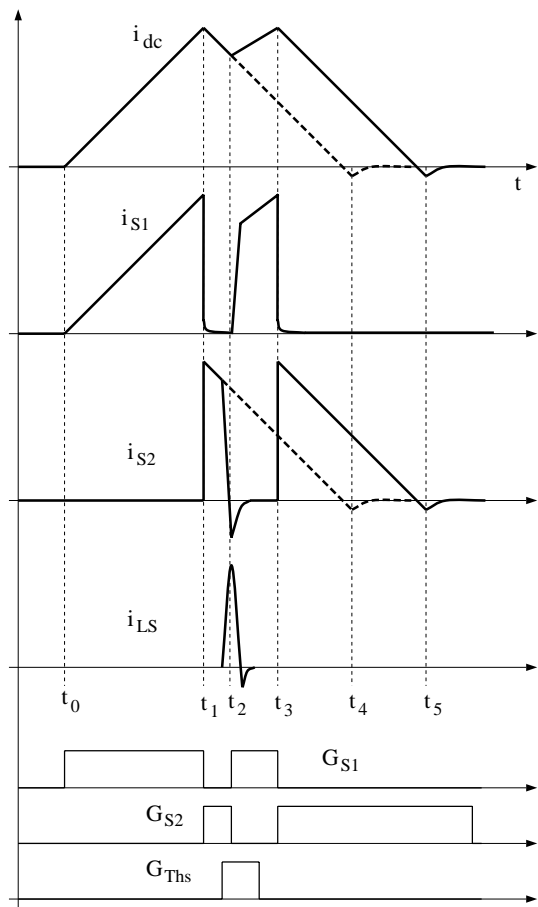


Fig. 6. High power (pulsed) test setup main waveforms.

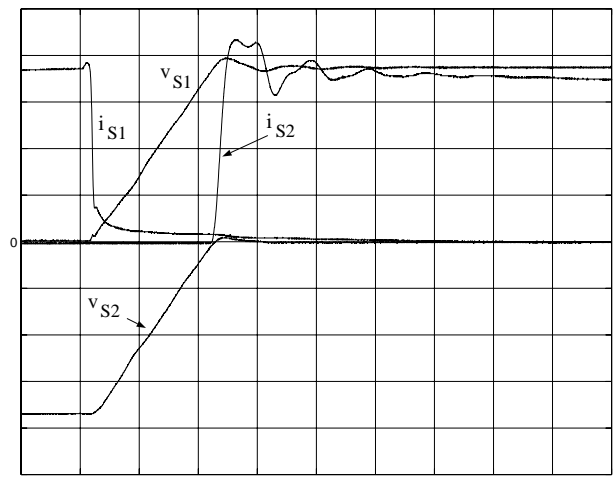
allows the use of larger snubber capacitors than in classical LRC snubbers, leading to significant reduction of the turn-off loss and better device utilization.

In fig. 7 the dV/dt across the device is about $75 \text{ V}/\mu\text{s}$. The voltage spike (and related power dissipation spike) across the device due to the stray inductances in the switch-snubber capacitor loop has been greatly reduced. The voltage overshoot shown in this figure is the voltage transient across the incoming switch due to combined effects of series stray inductance and the forward recovery process (significantly lower than the input voltage). The anode current peaking shown in fig. 7 has been observed and described earlier in the literature for GTO thyristors in resonant dc link converters [13]. The anode peaking phenomenon was explained as being caused by stray inductances causing transients in the anode-cathode voltage as the gate-cathode junction recovers its voltage blocking capability. Relevant turn-off data is summarized in Table I.

C.2 Turn-On process issues

The incoming switch S_2 enters conduction as soon as $v_{AK} > 0$. The overshoot in the current through S_2 is due to the stray inductance in series with the device and its forward recovery process (voltage overshoot followed by discharge of the snubber capacitor through the device).

The incoming switch is expected to start conducting at



Voltage scale: 200 V/div.
Current scale: 40 A/div.
Time base: 5 μs /div.

Fig. 7. Passive commutation sequence.

TABLE I

PASSIVE COMMUTATION - TURN-OFF DATA SUMMARY.

C_S [μF]	i_{dc} [A]	V_{in} [V]	E_{off} [mJ]	$t_{storage}$ [μs]	t_{fall} [μs]	$v_{ak_{max}}/V_{in}$ [V/V]
0.47	100	750	56	1.1	0.31	1.06
1.0	100	750	41	1.0	0.32	1.04
1.0	150	750	77	1.0	0.22	1.05
1.0	200	750	90	0.9	0.19	1.08

the zero crossing point of its anode-cathode voltage, provided that turn-on gate signals are supplied at a proper time. In this sense, it is desirable to apply the turn-on gate command to the incoming switch in advance, anticipating the zero crossing instant and minimizing the forward recovery losses. Positive current injection in gate G_1 while the MTO is still reverse biased takes the device into the far base transistor mode, operating in the active region. The current gain $|i_A|/i_{G_1}$ is strongly influenced by the anode voltage, that affects directly the $N - base$ width and the PNP transistor base transport factor (Early effect).

The effect of the anode voltage amplitude on the gain $|i_A|/i_{G_1}$ and the dynamics of the resonant snubber point out the trigger delay between the gate turn-on command of the incoming switch and the gate turn-off command of the outgoing switch, $\Delta t_g = t_{g,on} - t_{g,off}$, as a manipulation parameter to minimize the turn-on losses on the incoming switch due to transistor action and the forward recovery process. These energy loss terms as well as the total turn-on losses are shown in fig. 8, for $V_{in} = 600 \text{ V}$, $i_{dc} = 100 \text{ A}$ and $C_S = 1 \mu\text{F}$ as a function of Δt_g . A minimum turn-on energy point exists for given switching conditions. The dependence of the turn-on losses due to transistor action on the reverse anode voltage and considerations regarding simplification on the trigger timing and control logic, suggest $\Delta t_g = 0$ as the standard trigger delay.

A summary of relevant turn-on data obtained from the MTO-based test setup is listed in Table II ($\Delta t_g = 0$). The

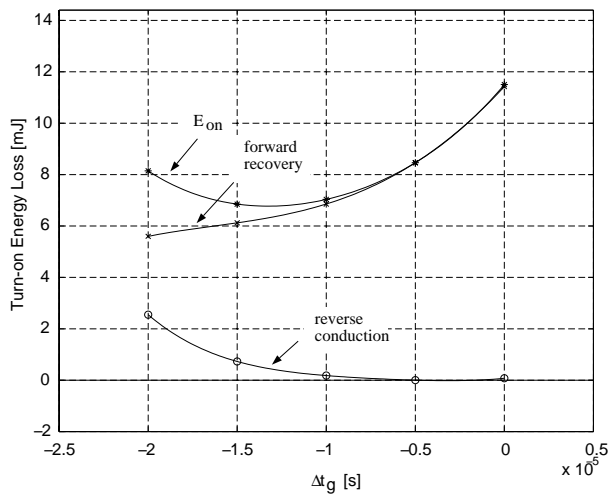


Fig. 8. Passive commutation: turn-on energy loss.

TABLE II
PASSIVE COMMUTATION - TURN-ON DATA SUMMARY.

C_S [μF]	i_{dc} [A]	V_{in} [V]	E_{on} [mJ]	di_A/dt [A/ μs]	$i_{A,max}/i_{dc}$ [A/A]
0.47	100	750	3	139	1.20
1.0	100	750	3	118	1.19
1.0	150	750	13	168	1.17
1.0	200	750	29	188	1.21

di_A/dt data in Table II has been evaluated at the point where $i_A = i_{dc}/2$.

It has been pointed out in the literature that the lack of a series inductor to limit the di_A/dt during the passive commutation sequence would limit the applicability of this snubber structure in converter circuits based on thyristor-type devices [6]. However, the di_A/dt data in Table II does not support the position above. In fact, the tests confirm the self limited di_A/dt characteristic of the MTO and, by extension, of GTO devices at turn-on, as pointed out by Wood [14]. The conclusion in this matter is that the lack of a series inductor does not constrain the application of the resonant snubbers with MTOs and possibly other thyristor-type devices with highly interdigitated gate-cathode structure. Low dI/dt rates result from the ZVS conditions implying a reduction of the α of the transistors in the MTO structure (wide neutral region in the N -base at low voltages), resulting in a less intense regenerative action and slower turn-on process.

D. Active Commutation

The active commutation sequence preserves the turn-on characteristics observed in the analysis of the passive commutation sequence. The main difference between the turn-on processes in these two commutation sequences is the magnitude of the reverse voltage across the incoming switch, significantly lower in the active commutation case. The turn-off process, on the other hand, is unique due to its zero current switching nature and the effects of the charge

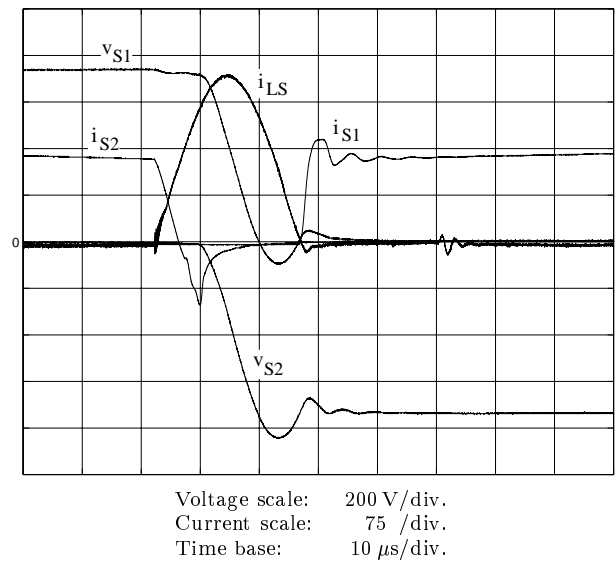


Fig. 9. Active commutation sequence: current boost mode.

stored in the outgoing switch over the commutation process.

The active commutation sequence starts as the snubber switch is turned on. Fig. 9 shows typical active commutation waveforms with the outgoing switch being turned-off under ZCS conditions. The switching conditions are such that $i_A \approx 150$ A, $v_{AK} = 750$ V, $C_S = 1.0$ μF .

D.1 Turn-off process issues

Fig. 9 shows that the reverse recovery waveforms are quite similar to the ones obtained for power thyristors. A difference is the presence of the anti-parallel diodes in the turn-off MOSFETs, limiting the reverse voltage across the gate-cathode junction to about -1 V. The gate-cathode voltage changing from the forward voltage drop (≈ 2 V) to the reverse clamp voltage causes the anode-cathode voltage to change by the same amount, resulting in transient current flow through the snubber capacitors.

The peak reverse recovery current I_{rr} and charge Q_{rr} under the conditions in fig. 9 are listed in Table III, as well as other relevant turn-off data. Large reverse recovery charge is observed in large devices such as the MTOs employed in this test setup. The reverse recovery charge of the outgoing switch is used to boost i_{L_S} to the magnitude required to compensate for losses during the resonant mode and guarantee ZVS conditions for the incoming switch (snubber energy boost). The portion of the reverse recovery current with positive derivative is associated with the turn-off losses in the outgoing switch, contributing to increase the losses during the resonant mode in the active commutation sequence.

The RMS factor presented in Table III can be reduced to the classical definition of the RMS value by multiplying the RMS factor by $1/\sqrt{T}$, where T is the switching period. This definition allows prompt evaluation of the RMS value of the snubber inductor current as well as the losses in the snubber inductor-switch branch for different switching frequencies.

TABLE III
ACTIVE COMMUTATION - TURN-OFF DATA.

	C_S [μF]	1.0
	L_S [μH]	11.3
	i_{dc} [A]	136
	V_{in} [V]	750
Snubber	$i_{L_{S_{peak}}}$ [A]	277
	RMS factor [$\text{A}\sqrt{\text{s}}$]	0.95
Turn-off	E_{off} [mJ]	75
	$v_{AK_{max}}/V_{in}$	1.13
	di_A/dt [$\text{A}/\mu\text{s}$]	-36
	I_{rr} [A]	-102
	Q_{rr} [μC]	356
	t_{rr} [μs]	7.0
	Softness factor	0.52

TABLE IV
ACTIVE COMMUTATION - TURN-ON DATA.

	C_S [μF]	1.0
	L_S [μH]	11.3
	i_{dc} [A]	136
	V_{in} [V]	750
Snubber	$i_{L_{S_{peak}}}$ [A]	277
	RMS factor [$\text{A}\sqrt{\text{s}}$]	0.95
Turn-on	E_{on} [mJ]	35
	$i_{a_{max}}/i_{dc}$	1.25
	di_A/dt [$\text{A}/\mu\text{s}$]	109

D.2 Turn-on process issues

The switching conditions as well as relevant turn-on data are listed in Table IV. A comparison between the turn-on losses computed for the passive and active commutation indicate higher losses for the latter one, under about the same operating conditions. This fact can be explained from the shorter interval between the instant when the incoming device is gated on ($v_{AK} < 0$, $dv_{AK}/dt < 0$) and the instant where it starts conducting ($v_{AK} \approx 0$, $dv_{AK}/dt > 0$) in the active commutation sequence. The turn-on process is slowed down further due to the reduction of the charge injected into the *P-base* and *N-base* regions of the device, increasing the turn-on losses. The dI/dt associated with the turn-on process in the active commutation as well as the peak anode current relative to the dc bus current are listed in Table IV.

IV. CONTROL CONSIDERATIONS

In order to guarantee zero voltage switching for the incoming switch, it is required to boost the snubber energy at the beginning of the resonant mode. The minimum amount of energy boost corresponds to the losses associated with the resonant mode in the active commutation sequence. Two strategies to boost the snubber energy have been proposed in the literature: the current boost and the voltage boost approaches [2], [3].

The current boost approach is based on delaying the

instant where the outgoing switch is turned off ($t = t_o^c$), so that $i_{L_S}(t_o^c) > i_{dc}$. The extra energy trapped in the snubber inductor at the beginning of the resonant mode corresponds to $(L_S I_{rr}^2)/2$ and it is strongly influenced by i_{dc} , $i_{L_S}(t_o)$ and di_{L_S}/dt . This strategy has been employed throughout this paper and is illustrated in fig. 9. The voltage boost approach is based on anticipating the turn-off instant of the outgoing switch, $t = t_o^v$, in order to obtain $i_{L_S}(t_o^v) < i_{dc}$. This condition results in boosting the snubber energy through an increase in the voltage on the snubber capacitors across the switches in the group undergoing commutation. An advantage of this latter strategy is the reduced dependence on the device Q_{rr} . Both snubber energy boost strategies can be obtained from the general solution for the resonant mode in the active commutation sequence [2]:

$$v_{C_{S_n}}(t - t_o) = Z_o[i_{dc} - i_{L_S}(t_o)] \sin\omega_o(t - t_o) + v_{L_S}(t_o) \cos\omega_o(t - t_o) - v_{L_S}(t_o) + v_{C_{S_n}}(t_o) \quad (2)$$

$$i_{L_S}(t - t_o) = \frac{1}{Z_o} v_{L_S}(t_o) \sin\omega_o(t - t_o) - [i_{dc} - i_{L_S}(t_o)] \cos\omega_o(t - t_o) + i_{dc} \quad (3)$$

where $\omega_o = 1/\sqrt{L_S C_{S_{eq}}}$ and $Z_o = \sqrt{L_S/C_{S_{eq}}}$, $C_{S_{eq}} = 3C_S$ for three-phase realizations and $C_{S_{eq}} = 2C_S$ for the commutation cell.

A detailed view of the turn-off process associated with the voltage boost mode is shown in fig. 10. As the outgoing device is turned off, the resonant mode is initiated. The voltage across both devices rise in the positive direction, increasing the energy in the snubber. As soon as the resonance brings the voltage on the outgoing device to negative levels, this device enters reverse conduction mode. The outgoing device continues in the reverse conduction mode until the excess carriers in junction j_1 are swept out by the reverse anode current. The gate-cathode junction does not enter avalanche breakdown due to the presence of the reverse diodes in the turn-off MOSFETs.

Large power devices always undergo a reverse recovery process in the active commutation sequence, independent of the turn-off method employed. This statement holds true for any design of the resonant snubbers of practical interest. Also, the relatively large switching times of large devices introduce additional uncertainty in the computation of the gate turn-off point leading to the desired snubber energy boost. In fact, the low dI/dt at gate turn-off shown in fig. 10 implies that a non-negligible amount of energy is dissipated instead of transferred to the snubber capacitors. These characteristics make the snubber current boost preferable when large, slow devices are employed in the main converter switches.

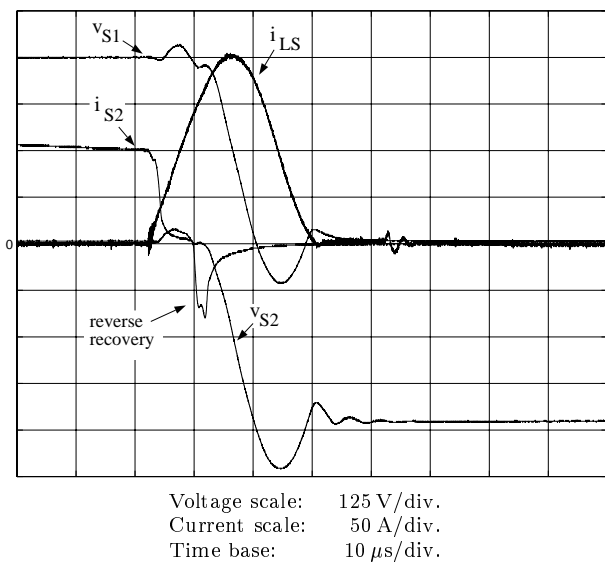


Fig. 10. Active commutation waveforms: snubber voltage boost.

V. TRADE-OFFS IN THE DESIGN OF THE RESONANT SNUBBERS FOR CSCs

A. Design of the snubber capacitor C_s

The critical dV/dt rating of the device employed in the main switches (rated at $1000 \text{ V}/\mu\text{s}$ for the MTO employed in this work) along with the maximum dc bus current defines a theoretical minimum size for the snubber capacitors. This rating, however, is generally related to the maximum dV/dt the device could be subjected to without re-triggering. A more restrictive constraint is introduced by the reduction of the switching losses, typically leading to capacitor sizes larger than those obtained from the critical dV/dt .

The minimum snubber capacitor size is set by the upper limit established for the turn-off energy loss during the passive commutation process. This reduction on the turn-off losses is obtained from the reduction of the dV/dt across the outgoing switch, lengthening the passive commutation interval for a given dc bus current. Detrimental effects of long commutation intervals include limitation of the PWM frequency and distortion of the AC waveforms, from comparatively large dwell times. Proper design of the snubber capacitor requires the use of experimental data relating the turn-off losses with the size of the snubber capacitor for given conditions of dc bus current and input voltage. Models approximating the turn-off characteristic of GTOs have been proposed in the literature [5] and can certainly be extended for MTOs given the similarities between these devices.

The placement of the snubber capacitor directly across the terminals of the power device introduces a second path for the current during the forward recovery process. As the forward voltage drop across the incoming device increases, due to the high device impedance in the initial stages of the turn-on process, the voltage across the snubber capacitor also increases. During this interval, part of the dc bus current is diverted through the snubber capac-

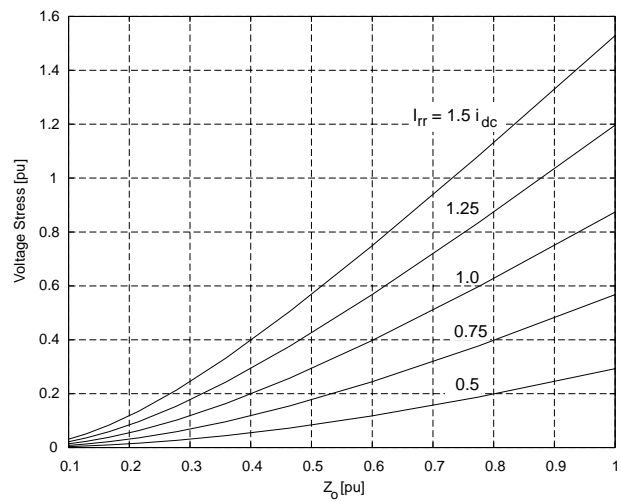


Fig. 11. Active commutation: voltage stress due to large I_{rr} .

itor. The resultant reduction of the magnitude of the current injected in the device during the initial stages of the forward recovery process contributes to augment the duration of this transient and to reduce the dI/dt at turn-on. As the impedance of the device drops rapidly causing v_{AK} to drop to the steady-state conduction level (conductivity modulation), the snubber capacitor discharge through the incoming device. The effects are an increase in the turn-on losses and current overshoot.

B. Design of the snubber inductor L_s

The snubber inductor design is aimed at the active commutation sequence. The basic design goal is to guarantee ZVS conditions for the incoming switch with minimum voltage and current stress on the main converter switches and snubber components.

The reverse recovery characteristics of the main power devices have significant impact on the performance of the resonant snubber. When the outgoing switch is turned off in ZCS mode, the snubber inductor current i_{L_s} is boosted by a magnitude corresponding to I_{rr} , increasing the energy stored in L_s . However, excessive boost of the snubber energy leads to higher voltage stress as the voltage on the snubber capacitor across the outgoing device is driven beyond the input voltage level. Fig. 11 shows computed plots of the extra voltage stress on the main switches as a function of the characteristic impedance Z_o of the resonant snubber for several values of I_{rr} . Low values of characteristic impedance are required to limit the overvoltage across the main switches. However, a reduction of the snubber inductor size increases the turn-off dI/dt (for a given input voltage), leading to larger I_{rr} and higher voltage and current stresses.

In this analysis, the base values are: $V_{base} = V_{L,RMS}$, $I_{base} = I_{L,RMS}$ and $Z_{base} = V_{base}/\sqrt{3}I_{base}$. The input voltage and dc bus current are assumed at maximum values for the purpose of stress estimation ($V_{in} = \sqrt{2}$ pu, $i_{dc} = \sqrt{2}$ pu). The estimates in fig. 11 are conservative since all losses were neglected.

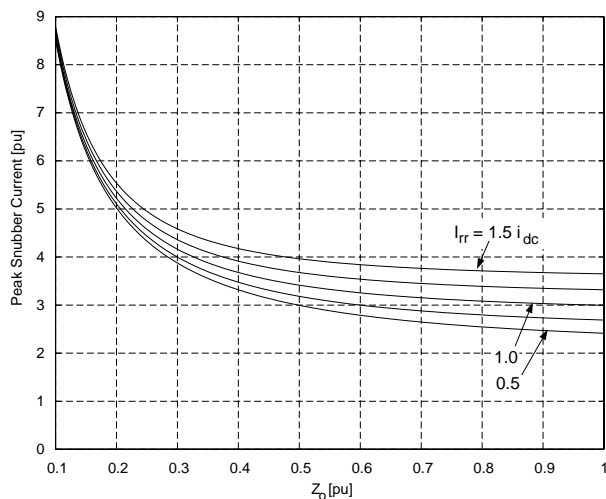


Fig. 12. Active commutation: current stress due to large I_{rr} .

Equally important as design quantities are the RMS and peak current levels through L_S . Since the snubber inductor and switch are series connected, the current through L_S also determines the current carrying characteristics required for the snubber switch Th_S . Here, the goal is to minimize the peak current through the snubber inductor relative to the dc bus current. The peak value of the snubber inductor current $i_{L_S,max}$ is reached during the resonant mode. From (3) $i_{L_S,max}$ is computed as:

$$i_{L_S,max} = \sqrt{\left(\frac{v_{L_S}(t_o)}{Z_o}\right)^2 + I_{rr}^2 + i_{dc}^2} \quad (4)$$

Fig. 12 illustrates the dependence of the peak snubber current on Z_o , for the same conditions employed in fig. 11. From fig. 12 it is clear that a compromise between the magnitude of the current through L_S , and consequently the losses on the snubber components, and the extra voltage stress on the main switches has to be established.

The turn-off loss on the outgoing switch is also a factor to be included in the design of L_S . From fig. 9 it is seen that the voltage across the outgoing switch is reapplied during the resonant mode in the active commutation process. The rate of decay of the reverse recovery current is determined by recombination inside this device as well as the formation of the depletion region. The reapplied dV/dt can be controlled through the natural resonance frequency of the snubber ω_o . Low values of ω_o are desirable to reduce the turn-off losses, but the commutation interval should be kept short for higher switching frequency capability.

VI. CONCLUSION

The impact of the switching characteristics of high power devices compatible with medium voltage CSC applications on the resonant snubber design and performance has been addressed in this paper.

A closer look into the MTO turn-off process reveals some limitations, mainly in hybrid devices: high sensitivity to stray inductances in series with the MOSFETs, intrinsic

limit on the maximum anode current that can be turned-off and potential for uneven current distribution at turn-off. These points determined the use of turn-off snubbers across the MTOs. In the test setup, the rate of reapplied voltage has been limited to $100 \text{ V}/\mu\text{s}$. Attempts to turn-off the devices at higher dv_{AK}/dt rates resulted in device failure at modest current and voltage levels ($200 \text{ A}/600 \text{ V}$).

The MTOs were observed to exhibit self-limited dI/dt at turn-on. In addition, the ZVS conditions contribute to slow down the turn-on process, reducing the current transfer ratio α of the transistors in the device structure ($di_A/dt < 200 \text{ A}/\mu\text{s}$ for dc bus currents up to 200 A). The trigger timing and reverse recovery characteristics of the main switches have been identified as important manipulation and disturbance quantities in the control of the commutation processes of the resonant snubber.

REFERENCES

- [1] W. McMurray, "Resonant snubbers with auxiliary switches," *IEEE Transactions on Industry Applications*, vol. 29, pp. 355-361, March/April 1993.
- [2] B. J. Cardoso and T. A. Lipo, "Current stiff converter topologies with resonant snubbers," in *IEEE Industry Applications Society Annual Meeting*, (New Orleans, Louisiana), pp. 1322-1329, October 1997.
- [3] B. J. Cardoso and T. A. Lipo, "A reduced parts count realization of the resonant snubbers for high power current stiff converters," in *IEEE Applied Power Electronics Conference*, (Los Angeles, California), pp. 558-564, March 1998.
- [4] B. J. Cardoso, S. Bernet, and T. A. Lipo, "A new control strategy for the PWM current stiff rectifier/inverter with resonant snubbers," in *IEEE Power Electronics Specialists Conference*, (Saint Louis, Missouri), pp. 573-579, June 1997.
- [5] H. Ohashi, "Snubber circuit for high power gate turn-off thyristor," *IEEE Transactions on Industry Applications*, vol. 19, pp. 655-664, July/August 1983.
- [6] J. Holtz, M. Stamm, J. Thur, and A. Linder, "High-power pulsewidth controlled current source GTO inverter for high switching frequency," in *IEEE Industry Applications Society Annual Meeting*, (New Orleans), pp. 1330-1335, October 1997.
- [7] D. E. Piccone, R. W. DeDoncker, J. A. Barrow, and W. H. Tobin, "The MTO thyristor - A new high power bipolar MOS thyristor," in *IEEE Industry Applications Society Annual Meeting*, pp. 1472-1473, October 1996.
- [8] D. E. Piccone and et al., "MTO thyristor." Application Notes, SPCO, Fall 1997.
- [9] R. Rodrigues, D. Piccone, A. Huang, and R. DeDoncker, "MTO thyristor power switches," in *Power Systems World Conference Records*, (Baltimore, Maryland), pp. 3.53-3.64, September 1997.
- [10] B. J. Baliga, *Power Semiconductor Devices*. PWS Publishing, 1996.
- [11] D. F. Grafham and F. B. Golden, *SCR Manual including Triacs and other thyristors*. Reward Books, 1979.
- [12] R. W. DeDoncker and J. P. Lyons, "The auxiliary resonant commutated pole converter," in *IEEE Industry Applications Society Annual Meeting*, pp. 1228-1235, October 1990.
- [13] G. L. Skibinski and D. M. Divan, "Characterization of GTO for soft switching applications," in *IEEE Industry Applications Society Annual Meeting*, pp. 638-646, October 1988.
- [14] P. Wood, *Fundamentals and applications of Gate-Turn-Off thyristors*. EPRI, 1988.